

# The Redshift Distribution and Luminosity Functions of Galaxies in the Hubble Deep Field

Stephen D. J. Gwyn and F. D. A. Hartwick

Department of Physics and Astronomy, University of Victoria,  
Box 3055, Victoria, British Columbia, V8W 3P6, Canada  
gwyn, hartwick@uvastro.phys.uvic.ca

## ABSTRACT

Photometric redshifts have been determined for the galaxies in the Hubble Deep Field. The resulting redshift distribution shows two peaks: one at  $z \sim .5$  and one at  $z \sim 2.5$ . Luminosity functions derived from the redshifts show strong luminosity evolution as a function of redshift. This evolution is consistent with the Babul & Rees (1992) scenario wherein massive galaxies form stars at high redshift while star formation in dwarf galaxies is delayed until after  $z = 1$ .

*Subject headings:* galaxies: distances and redshifts — galaxies: formation — galaxies: photometry

## 1. Introduction

The Hubble Deep Field <sup>1</sup> (HDF) optical images are the deepest yet obtained (Williams et al., 1996). Objects as faint as  $I_{ST}=28.5$  <sup>2</sup> can be detected at the  $10\sigma$  level. At this point in time, no spectroscopic redshifts have been measured for the faintest galaxies in these images.

Photometric redshifts (see, for example, Gwyn, 1995; Connolly et al., 1995; Koo, 1985) can be measured much faster and to much fainter magnitudes than their spectroscopic counterparts. Because the wavelength bin-size in photometry is generally so much larger than in conventional spectroscopy ( $\sim 1000\text{\AA}$  *vs.*  $1\text{--}2\text{\AA}$ ), far shorter exposure times are required to measure redshifts (but with a sacrifice in accuracy).

---

<sup>1</sup>Based on observations with the NASA/ESA *Hubble Space Telescope*, obtained at the Space Telescope Science Institute, which is operated by AURA, under NASA contract NAS 5-26555.

<sup>2</sup>for simplicity,  $U_{ST}, B_{ST}, R_{ST}$  and  $I_{ST}$  will be used to denote magnitudes in the F300W, F450W, F606W and F814W bands respectively. The ST zero-point system is used unless otherwise specified.

Photometric redshifts have been calculated for the galaxies brighter than  $I_{ST} = 28$  in the Hubble Deep Field. This paper presents the redshift distribution for this sample. Also presented are luminosity functions as a function of redshift out to  $z = 5$ .

## 2. The photometric redshift technique

The photometric redshift technique can be divided into three steps: First, the photometric data for each galaxy in the fields are converted into spectral energy distributions (SED's). Second, a set of template spectra of all Hubble types and redshifts ranging from  $z = 0$  to  $z = 5$  is compiled. Third, the spectral energy distribution derived from the observed magnitudes of each object is compared to each template spectrum in turn. The best matching spectrum, and hence the redshift, is determined by minimizing  $\chi^2$ . In the following subsections, each of these steps is examined.

### 2.1. Photometry to spectral energy distributions

The magnitude in each bandpass is converted to a flux (power per unit bandwidth per unit aperture area) at the central or effective wavelength,  $\lambda_{cen}$ , of the bandpass. When the flux is plotted against wavelength for each of the bandpasses, a low resolution spectral energy distribution is created.

The following equation converts magnitudes in some filter,  $f$ , to fluxes:

$$F_f = F_0 10^{-m_f/2.5}, \quad (1)$$

where  $m_f$  is the apparent magnitude,  $F_f$  is the flux in units of  $\text{W } \text{\AA}^{-1} \text{ m}^{-2}$  and  $F_0$  is the flux zero-point of that filter system in the same units. This equation is simple to use as long as the flux zero-point is known. Unlike almost all other magnitude systems (*e.g.* the Johnson/Cousins UBVRI system) the flux zero-points for the ST magnitude system are the same for all filters, making the conversion of magnitudes to fluxes straightforward.

### 2.2. The template spectra

The template spectra were produced from the models of Bruzual & Charlot (1993). They showed that their models faithfully reproduce the spectra of local galaxies. More recently, Steidel et al. (1996) found that high redshift galaxies are also well described by the models. To represent the different galaxy types at a given redshift, an interpolation was made between

the instantaneous burst model (for early-type galaxies) and the constant star formation rate model (for late-type galaxies) of Bruzual & Charlot (1993). These interpolated spectra were redshifted from  $z = 0$  to  $z = 5$ .

To compare the template spectra with the SED’s of the observed galaxies, the redshifted spectra were reduced to the passband averaged fluxes  $F_{pb}$  at the central wavelengths of the passbands:

$$F_{pb} = \frac{\int_{\lambda_1}^{\lambda_2} T(\lambda) P(\lambda) d\lambda}{\int_{\lambda_1}^{\lambda_2} P(\lambda) d\lambda}, \quad (2)$$

where  $P(\lambda)$  is the response function of the passband and  $\lambda_1$  and  $\lambda_2$  represent the wavelengths where the passband response function falls to zero.

### 2.3. Comparing the templates to the SED’s

Given a spectral energy distribution of a galaxy of unknown redshift and a set of templates, the next step is to compare the SED to each of the templates in turn and to the template which most closely matches the SED. The degree to which each template matches the observed SED is quantified in the following manner:

$$\chi^2 = \sum_{i=1}^{N_f} \frac{(F_i - \alpha T_i)^2}{\Delta F_i^2}, \quad (3)$$

where  $N_f$  is the number of filters in the set,  $F_i$  and  $\Delta F_i$  are respectively the flux and the uncertainty in the flux in each bandpass of the observed galaxy,  $T_i$  is the flux in each bandpass of the template being considered, and  $\alpha$  is a normalization factor. A normalization factor is necessary to compare properly the galaxies and the templates because the fluxes of the galaxies are very small relative to the fluxes of the templates. Each template is then compared to the target galaxy SED and the smallest value of  $\chi^2$  is found. The best matching template gives  $z_{phot}$ , the sought-after photometric redshift of the galaxy.

## 2.4. Accuracy

The photometric redshift technique has been tested with simulations and photometric observations of galaxies with known spectroscopic redshifts.

The simulations take the following form: A spectral energy distribution is chosen from the template SED's available. The SED is reduced to fluxes at the central wavelength of the passbands of the filter set to be tested. To simulate observational errors, a small random number with a Gaussian distribution is added to the fluxes in each band of the chosen template. Photometric redshifts are determined from the resulting simulated photometry in the manner described above. These photometric redshifts are compared with the redshifts of the templates from which they were derived.

Not surprisingly, when the errors in the photometry are zero, the photometric redshift technique always picks the correct redshift. As the errors in the photometry increase, so do the errors in the photometric redshifts in the form of the standard deviation of redshift residuals.

The technique was also tested using a number of samples of galaxies with known (spectroscopic) redshifts: the Colless et al. (1990, 1993) sample, the Bershady et al. (1994) sample and the Canada-France Redshift Survey (Lilly et al., 1995a). Multi-colour photometry is available for these samples: *BVRI*, *UJFNK* and *BVIK* respectively. By comparing the redshifts derived from this photometry with the spectroscopic redshifts, it is possible to determine the accuracy of photometry redshift technique.

The accuracy of the observed photometric redshifts closely follows the predictions of the simulations. This indicates that the simulations are a reasonable representation of reality, an important point because, as of yet, there is no spectroscopic redshift/multi-colour photometry sample using the F300W, F450W, F606W and F814W filters. Consequently, no empirical photometric/spectroscopic redshift comparison has been performed to determine the uncertainties associated with the photometric redshift for the HDF filters. One must therefore rely on the simulations to determine the uncertainties. The simulations show that the uncertainties in the photometric redshifts,  $\sigma_{pz}$ , increase with redshift. For  $z < 1$  they are only  $\sigma_{pz} \simeq 0.07$ ; for  $1 < z < 3$  they are  $\sigma_{pz} \simeq 0.12$  and for  $3 < z < 5$  they are  $\sigma_{pz} \simeq 0.20$ .

As further check on the photometric redshift technique, the two-colour criterium of Steidel, Pettini & Hamilton (1995) was applied to the sample. They found that galaxies with a red  $U_n - G$  color and a blue  $G - R$  color were at  $3.0 \lesssim z \lesssim 3.5$  where the filters straddle the Lyman 912Å break. The  $U_{ST}B_{ST}R_{ST}$  filter system is somewhat different than the  $U_nGR$  system; it straddles the break at a slightly different redshift. However, virtually all (99%) of the galaxies with  $U_{ST} - B_{ST} > 0$  and  $B_{ST} - R_{ST} < 0$  were at redshifts greater than  $z \sim 2$ .

### 3. The redshift distribution and luminosity function

The positions of the galaxies in the HDF images were taken from the catalogs of Couch (1996). Magnitudes were measured for all galaxies through a 0.2 arc-second radius aperture. The photometric redshift technique was used on all galaxies brighter than  $I_{ST} > 28$ . Because some galaxies have no  $U_{ST}$  magnitudes, redshifts can only be measured for 90% of the galaxies. The redshift distribution is shown in Figure 1. The distribution shows two peaks, one at a redshift of about  $z \simeq 0.5$  and another at  $z \simeq 2.5$ .

Compared to spectroscopic redshifts, where typically  $\Delta z \sim 0.001$ , the uncertainties associated with photometric redshifts are large. Note, however, that the width of the bins in this histogram (0.2 in  $z$ ) are comparable to the errors expected in the photometric redshifts ( $\sigma_{pz} \lesssim 0.2$ ). Simulations indicate that this level of precision is sufficient to calculate accurate luminosity functions. Indeed, photometric redshifts have been used at  $z \sim .35$  to calculate LF's identical to those determined using spectroscopic redshifts (Gwyn, 1995).

The luminosity functions (LF's) were constructed using the  $1/V_a$  method. The  $1/V_a$  method is well known and has been described in detail elsewhere (Schmidt, 1968, Lilly et al., 1995b) so the following description is brief.

$V_a$  is defined as the volume accessible to a galaxy given its absolute magnitude and the limits defining the sample in which it is found. Formally,

$$V_a = \int_{z_{min}}^{z_{max}} \frac{dV}{dz} dz, \quad (4)$$

where  $dV/dz$  is the co-moving differential volume element. The limits,  $z_{min}$  and  $z_{max}$  can be fixed (as in a volume limited sample), but for a magnitude limited sample they must be determined for every galaxy. Given the absolute magnitude,  $M$ , of each galaxy and the limiting apparent magnitude of the sample,  $m_{lim}$ , the limiting redshift at which the galaxy would still be in the sample,  $z_{lim}$ , can be determined. The luminosity function,  $\Phi$ , is the sum of the inverse of the accessible volumes ( $\sum 1/V_a$ ) normalized to the angular area surveyed.

The luminosity function was calculated for three redshift regions:  $z < 1$ ,  $1 < z < 3$  and  $3 < z < 5$ . In each case,  $z_{min}$  was the lower bound of each redshift region ( $z = 0, 1$  and  $3$  respectively). The minimum of the upper bound of each redshift region ( $z = 1, 3$  and  $5$  respectively) or  $z_{lim}$  (as determined for each galaxy using  $I_{ST} = 28.0$  for  $m_{lim}$ ) was used for  $z_{max}$ . A cosmology where  $H_0 = 75$  km sec $^{-1}$  Mpc $^{-1}$ ,  $\Omega_0 = .3$ , and  $\lambda_0 = 0$  is assumed.

The luminosity functions thus calculated are shown in Figure 2. In order to compare the luminosity functions with local LF's, they are shown in the (Johnson)  $B$  band. Note that it is not necessary when using the  $1/V_a$  method to use the same filter to calculate both

the  $V_a$ ’s and the absolute magnitudes.

Shown for comparison as a solid line is the local luminosity function of Loveday (1992). The lowest redshift division ( $z < 1$ , dotted line) shows the steep faint end of the local luminosity function. The next highest redshift division ( $1 < z < 3$ , dashed line) lacks this faint tail; the space density of faint galaxies seems depressed with respect to the local LF. The bright end is about 4 magnitudes brighter than the local luminosity function. The bright end is fainter by about 1.5 magnitudes in the highest redshift interval ( $3 < z < 5$ , dot-dashed line). Although different cosmologies change the positions (and, to a lesser degree, the shape) of the luminosity functions, changing the parameters does not greatly alter the relative positions of the LF’s at various redshifts to one another.

These variations in the luminosity function with redshift can be explained if there are two epochs at which galaxies undergo their first major burst of star formation. The first occurs before  $z \gtrsim 2.5$ ; at this time the larger galaxies start forming stars. The galaxies do not all burst simultaneously. The stars of some galaxies first turn on at  $z \sim 5$ , some form as late as  $z \sim 2$  while most form at  $z \sim 2.5$ , corresponding to the peak of the redshift distribution shown in Figure 1. Depending on the fraction of gas that is converted into stars in the initial starburst, a fading of 4 magnitudes since  $z \sim 2.5$  is entirely consistent with the Bruzual & Charlot (1993) models.

In the Babul & Rees model (Babul & Rees, 1992; Babul & Ferguson, 1996), the star formation in dwarf galaxies is delayed until  $z \sim 1$  by photoionization of their gas by intergalactic ultraviolet radiation. This second epoch of star formation explains the observed excess at moderate redshifts of faint blue galaxies (termed “boojums” for “blue objects observed just undergoing moderate starburst” by Babul & Rees, 1992). These galaxies end up on the steeply rising faint tail of the lowest redshift luminosity function. This scenario would also explain why the higher redshift luminosity functions in Figure 2 have depressed faint ends: the galaxies that would populate the faint end haven’t turned on yet.

#### 4. Summary

Using photometric redshifts, a redshift distribution has been determined for the Hubble Deep Field. It shows two peaks: one at  $z \simeq 0.5$  and another at  $z \simeq 2.5$ . Luminosity functions have been calculated using these redshifts. The LF’s show strong evolution: the brightest galaxies are 4 magnitudes brighter than their present day counterparts and the faint galaxies are fewer in number. The double-peaked redshift distribution and the evolution of the luminosity function can be understood if larger galaxies form stars early at  $z \sim 3$  and if

star formation is delayed in the dwarf galaxies until after  $z \simeq 1$ .

Thanks are due to D. Crampton for suggesting the application of our photometric redshift technique to the Hubble Deep Field. F.D.A.H. gratefully acknowledges financial support for this project through an NSERC operating grant.

## REFERENCES

Babul, A. & Ferguson, H. C. 1996, ApJ, 458, 100

Babul, A. & Rees, M. J. 1992, MNRAS, 255, 364

Bershady, M. A., Hereld, M., Kron, R. G., Koo, D. C., Munn, J. A., & Majewski, S. R. 1994, AJ, 108, 870

Bruzual, G. A. & Charlot, S. 1993, ApJ, 405, 538

Colless, M. M., Ellis, R. S., Broadhurst, T. J., & Peterson, B. A. 1993, MNRAS, 244, 408

Colless, M. M., Ellis, R. S., Taylor, K., & Hook, R. N. 1990, MNRAS, 244, 408

Connolly, A. J., Csabai, I., Szalay, A. S., Koo, D. C., Kron, R. G., & Munn, J. A. 1995, AJ, 110, 2655

Couch, W. J. 1996, Public communication, [<http://ecf.hq.eso.org/hdf/catalogs>]

Gwyn, S. D. J. 1995, unpublished Master's thesis, University of Victoria

Koo, D. C. 1985, AJ, 90, 418

Lilly, S. J., Fèvre, O. L., Crampton, D., Hammer, F., & Tresse, L. 1995a, ApJ, 455, 50

Lilly, S. J., Tresse, L., Hammer, F., Crampton, D., & Fèvre, O. L. 1995b, ApJ, 455, 108

Loveday, J., Peterson, B. A., Efstathiou, G., & Maddox, S. J. 1992, ApJ, 390, 338

Schmidt, M. 1968, ApJ, 151, 393

Steidel, C. C., Giavalisco, M., Pettini, M., Dickinson, M., & Adelberger, K. L. 1996, Preprint [astro-ph/9602024]

Steidel, C. C., Pettini, M., & Hamilton, D. 1995, AJ, 110, 2519

Williams et al. 1996, to be published in *Science with the Hubble Space Telescope— II*, P. Benvenuti, F. D. Macchetto, & E. J. Schreier, eds. (Baltimore: STScI), p. 390

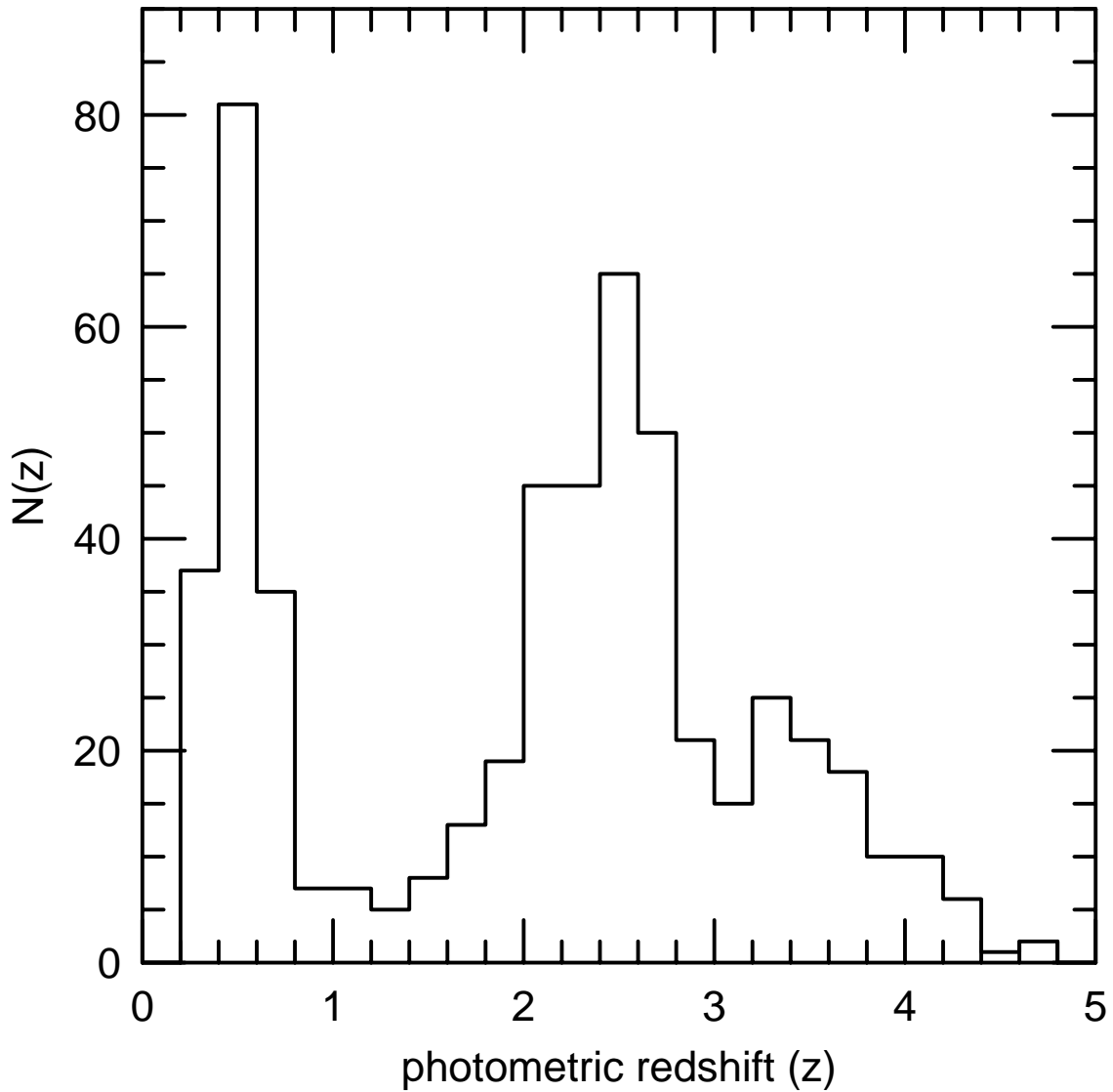


Fig. 1.— The HDF redshift distribution. Two peaks are visible in the distribution: one at  $z \sim .5$  and one at  $z \sim 2.5$ .

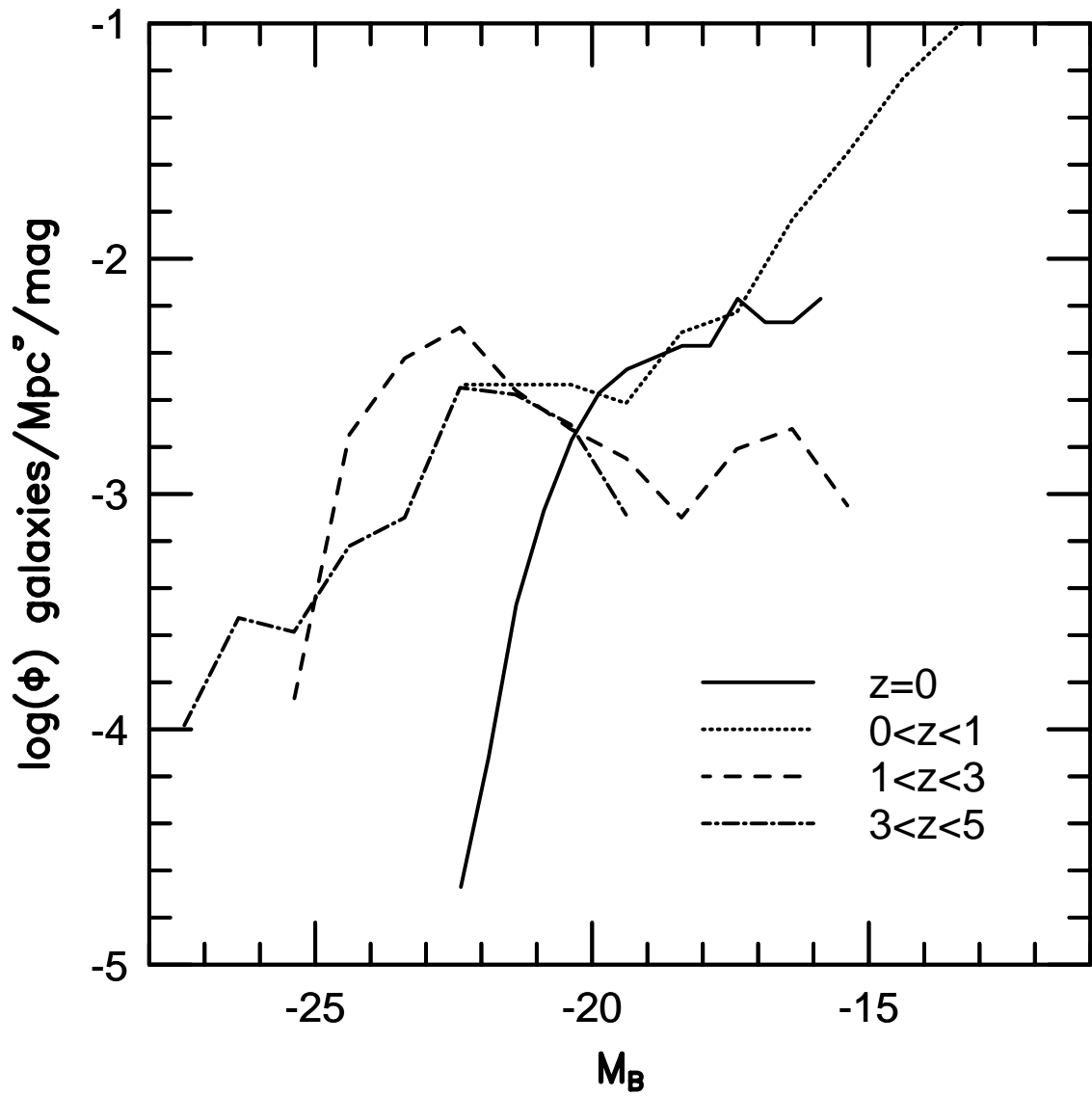


Fig. 2.— The evolution of the (Johnson)  $B$  luminosity function with redshift. The local LF is that of Loveday et al. (1992).